Korean J. Chem. Eng., 33(7), 2073-2083 (2016)
DOI: 10.1007/s11814-016-0048-z

pISSN: 0256-1115
eISSN: 1975-7220

Investigation of synergistic adsorption between methyl orange and Cd(II) from binary mixtures on magnesium hydroxide modified clinoptilolite

Weihua Zou*,†, Lie Liu,†, Hongping Li*, and Xiuli Han***

*School of Chemical Engineering and Energy, Zhengzhou University, 100# of Kexue Road, Zhengzhou 450001, P. R. China
**College of Public Health, Zhengzhou University, 100# of Kexue Road, Zhengzhou 450001, P. R. China
(*Received 7 January 2015 • accepted 18 February 2016*)

Abstract−The simultaneous removal of Methyl orange (MO) and Cd^{2+} (mainly from organo-metallic dyes) onto magnesium hydroxide modified clinoptilolite (MHMC) was described and compared to a single adsorbate situation. The adsorption performance was studied by batch experiments. The adsorption mechanism of MO and Cd^{2+} on MHMC was investigated. Langmuir and Dubinin-Raduskevich (D-R) isotherm successfully predicted the adsorption of MO and Cd^{2+} in single and binary systems. Maximum adsorption capacity calculated from Langmuir isotherm equation in single solution for MO and Cd^{2+} was 0.305 and 0.282 mmol/g, respectively. In a binary system of MO/Cd^{2+}, the adsorption capacity for both MO and Cd^{2+} was higher than in single solutions. The results indicated that the adsorption system of MO/Cd^{2+} presented a synergistic effect, not competitive adsorption, which suggested that MHMC can be used as an adsorbent for removal of dyes and heavy metal in the multi-solute system.

Keywords: Magnesium Hydroxide Modified Clinoptilolite (MHMC), Adsorption, Isotherms, Kinetics, Methyl Orange, Cd^{2+}

INTRODUCTION

Wastewater containing dye and heavy metal ions from dyestuff and textile industries is one of difficult industrial wastewaters to treat or dispose of. Dyes and heavy metal ions are important pollutants, causing environmental and health problems to humans and aquatic animals. Dyes can be classified as anionic (direct, acid and reactive dyes), cationic (basic dyes) and non ionic (disperse dyes) [1]. Removal of many reactive azo dyes from textile wastewater is difficult because of their highly solubility in water, complex structure and synthetic origin [2]. Heavy metals have harmful effects on human physiology and other biological systems when they exceed tolerance levels, which are generally in the level of less than one part per million (ppm) [3]. Therefore, the removal of dyes and heavy metals from wastewater before discharging to the environment is important. Adsorption has been recognized as a conventional process for the removal of dyes and heavy metals from effluents [4,5] because of its chemical stability, high efficiency, high selectivity, facility of employment, wide range of available adsorbents and economic feasibility.

In recent years, due to the environmentally benign nature, excellent adsorption properties and low cost, metal oxide or metal hydroxide as the materials for water treatment have caused more and more widespread concern [6]. Magnesium hydroxide has a high surface free energy with a large adsorptive surface area and a positive surface charge, it can be used to attract negatively charge ions such as anionic dyes. It also can be used as a neutralizing agent for some wastewater steams [7]. However, the fine particle size of the magnesium hydroxide makes it very difficult to separate from the water phase, which limits its application in wastewater treatment. But coating magnesium hydroxide to a media surface may provide an effective surface and may be a promising medium for dyes and heavy metal removal from wastewater [8]. The clinoptilolite coated with a layer of magnesium hydroxide can not only overcome their respective shortcomings, but also enhance sorption capacity of clinoptilolite because of bigger surface area and stronger ion exchange capacity. To our best knowledge, little study has been reported to use the magnesium hydroxide modified clinoptilolite as adsorbent and investigate the effects of dye and heavy ion on the adsorption performance of magnesium hydroxide modified clinoptilolite so far.

Within literature a large number of research papers have considered adsorption processes for the single component systems (dye or metal ion) [9-16]. However, most industrial effluents contain a mixture of several dyes; moreover, in the wastewater of pigments industries, paints, paper manufacturing and automobile production, heavy metals are also present with dyes. Since some dyes are toxic, nondegradable, stable and even carcinogenic, the treatment of these wastewaters is very difficult and mostly ineffective when using traditional purification processes [17]. But few studies have focused on the simultaneous removal of dyes and metal ion in multiple systems. Meanwhile, the nature of adsorption mechanism has been inadequately understood. So it is necessary to study the simultaneous adsorption process involving two or more components because sole dye or toxic metal ions rarely exist in wastewater [18].

In this paper, magnesium hydroxide modified clinoptilolite (MHMC) was used as an adsorbent for removal of Cd^{2+} and Methyl orange (MO) (Scheme 1) from single and binary solutions. Hence,

†To whom correspondence should be addressed.
E-mail: whzou@zzu.edu.cn, whzou@163.com

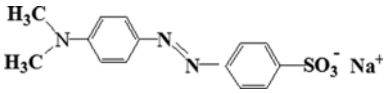

Scheme 1. The structure of Methyl orange (MO).

the objectives of the study were to assess adsorption behavior of Cd^{2+} and MO in single and binary systems toward MHMC, determine the simultaneous removal properties for Cd^{2+} and MO by MHMC through isotherm and kinetic modeling; and understand the adsorption mechanism and components associated with removal of Cd^{2+} and MO.

MATERIALS AND METHODS

1. Adsorbent Preparation and Characterization

Nature clinoptilolite (NC) samples were taken from Xinyang City, P. R. China. The clinoptilolite was sieved to obtained average size particles about 20-40 mesh and washed several times by distilled water and dried at 378 K in an oven for 24 h. The dry clinoptilolite was stored for surface coating. Then, the magnesium hydroxide emulsion was synthesized by using magnesium chloride and ammonia with a definite $MgCl_2/NH_3$ mole ratio of 1 : 2. Next, 50 g clinoptilolite and 100 mL magnesium hydroxide emulsion were mixed with slight stirring. Later, the mixture was placed in a muffle furnace and keeping 378 K for 5 h. Finally, the mixture was cooled to room temperature and washed to pH 8.50 using distilled water. Last, the sample of MHMC was dried at 378 K and stored in airtight container for use.

Photomicrography of the exterior surface of NC and MHMC was obtained by JSM-7500 F (Japan) scanning electron microscope (SEM). The functional groups present in NC and MHMC were characterized by a Fourier transform infrared spectrometer (PE-1710, USA), using potassium bromide discs to prepare the NC and MHMC samples. The spectral range varied from 4000-400 cm^{-1}. The mineralogy of the sample was characterized by X-ray diffraction (XRD) (Tokyo ShibauraModel ADG-01E). The pH of zero point charge (pH_{pzc}) was obtained to evaluate the MHMC surface charge at different pH and the pH_{pzc} was found to be 8.61. The pH_{pzc} of the MHMC was determined according to reference [19].

2. Adsorbate

Anionic dye (MO with 99% purity) was used to test the adsorption capacity of MHMC without further purification. The dye stock solutions were prepared by dissolving accurately weight dyes into deionized water to desired concentration. The stock solution of Cd^{2+} was prepared from $Cd(NO_3)_2{\cdot}4H_2O$ (analytical grade) in deionized water, and to prevent the precipitation of Cd^{2+} by hydrolysis, the stock solution of Cd^{2+} contained a few drops of 0.1 mol/L HNO_3. The experimental solutions were obtained by diluting the stock solutions in accurate proportions to different initial concentrations. The initial pH of the working solution was adjusted by adding a small volume of 1.0 mol/L HCl or 1.0 mol/L NaOH solution and monitored by a pH meter.

3. Adsorption Experiments

3-1. Adsorption Isotherms

The adsorption of MO and Cd^{2+} by MHMC in single and binary systems was performed by a batch equilibrium technology at 298 K. For single adsorption system, a series of 125 mL Erlenmeyer flasks with 2.0 g/L of MHMC and 10 mL solution at different initial concentrations were shaken by the thermostat-shaking equipment at 100 rpm for 360 min. The initial concentration of MO and Cd^{2+} varied from 0.153 to 1.833 mmol/L and 0.178 to 2.590 mmol/L, respectively. The initial solution pH value was adjusted with 1.0 mol/L NaOH or HNO_3 solutions. After adsorption, the pH values of the solution were also analyzed, and the variations were all within one unit.

For binary adsorption system, the initial concentrations of the target species MO varied over the range of 0.153-1.833 mmol/L with a pH level of 7.0, which is the same phenomenon as the initial concentrations in single adsorption system. In the mixture solutions, the initial concentration of the interferential species Cd^{2+} was fixed at 0.604, 0.893 or 1.227 mmol/L, respectively. Similarly, the initial concentrations of the target species Cd^{2+} varied over the range from 0.178 to 2.590 mmol/L, while the initial concentration of the interferential species MO was fixed at 0.603, 1.033 or 1.242 mmol/L in the binary systems, respectively.

3-2. Adsorption Kinetics

The kinetic experiments involved the same method as described earlier, except that the samples were collected at predetermined time intervals to determine the adsorption equilibrium time.

For a single component system, a series of 125 mL flask with 2.0 g/L of MHMC and 10 mL MO or Cd^{2+} solution at the same initial concentrations of 1.2 mmol/L were shaken at 298 K. The flasks were then taken out at predetermined time intervals. For binary adsorption system, MHMC at loadings of 2.0 g/L was mixed with MO and Cd^{2+} mixture solution at the same initial concentrations (0.6 mmol/L).

4. Analytical Methods

The concentration of MO that remained in solutions as the residual dye after adsorption was determined using a UV spectrophotometer (Shimadzu UV-3000) at λ_{max} 463 nm, and the concentration of Cd^{2+} was measured by AAanalyst 300 flame atomic absorption spectrometer at λ_{max} 228.8 nm. Since the λ_{max} of dye solution might shift to different wavelength, particularly at different pH, the pH of diluted residual solutions was fixed at pH 7.0 before measuring the absorbance.

The adsorption capacity of MHMC at equilibrium (q_e, mmol/g) and at time t (q_t, mmol/g) was calculated with Eq. (1) and Eq. (2). The equilibrium distribution coefficient (K_d, mmol/L) could be determined with Eq. (3).

$$q_e = \frac{(C_0 - C_e)v}{m} \quad (1)$$

$$q_t = \frac{(C_0 - C_t)v}{m} \quad (2)$$

$$K_d = q_e/C_e \quad (3)$$

where v (L) is the volume of adsorbate solution, C_0 (mmol/L) is the initial concentration of adsorbate, C_t (mmol/L) is the concentration of adsorbate at a given time t, C_e (mmol/L) is the equilibrium concentration of adsorbate at equilibrium and m (g) is the dry weight of the adsorbents. K_d is the equilibrium distribution

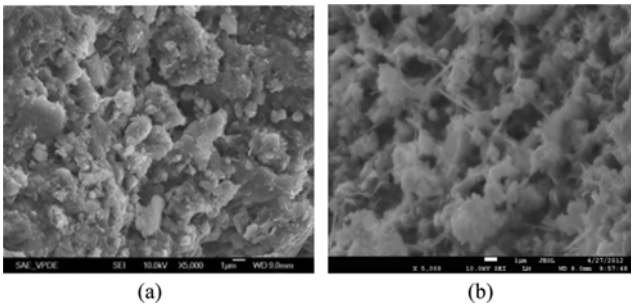

Fig. 1. SEM of NC (a) and MHMC (b).

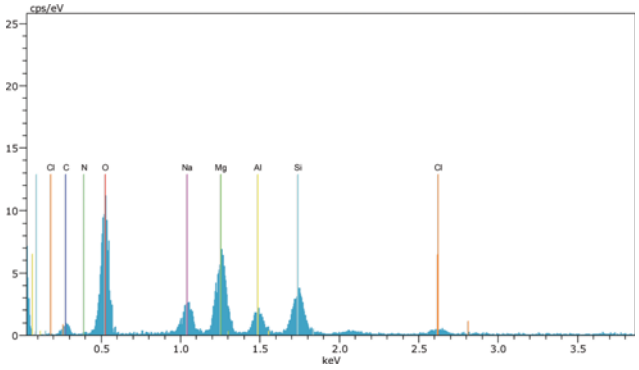

Fig. 2. EDAS spectra of modified clinoptilolite.

coefficient (mmol/L). All the adsorption experiments were conducted in triplicate, and the mean values were presented.

RESULTS AND DISCUSSION

1. Characterization of NC and MHMC

1-1. SEM Observations and EDAX Analysis

The sample of clinoptilolite coated with magnesium hydroxide was white colored precipitate, indicating the presence of magnesium hydroxide in the form of insoluble hydroxide. SEM observation reported in Fig. 1 showed the porous structure of NC and MHMC (5000×enlargement). It can be seen that the NC's surface texture was irregular. Comparing the images of NC, the MHMC's surface did not grow randomly but was homogeneously distributed on the surface. In conjunction with electron microscopy, elemental identifications of surface features were performed by qualitative EDAX analysis. The EDAX results are the following: there are O (48.10%), Mg (0.52%), Al (6.21%), Si (40.21%), in surface of clinoptilolite by EDAX analysis, while O (50.86%), Mg (14.47%), Al (4.78%), Si (9.56%) in surface of MHMC (Fig. 2). The EDAX analysis yielded direct evidence for magnesium hydroxide coated on the surface of clinoptilolite.

1-2. FTIR Analysis

The FT-IR spectrum of NC and MHMC is shown in Fig. 3. The FTIR spectra of clinoptilolite were composed of the peaks of sorbed water, vibration of framework of Si-O or Al-O [8]. Compared to FTIR of clinoptilolite, the spectra of MHMC can be matched with the spectrum of the virgin clinoptilolite, with additional peaks detected at 1,400 cm^{-1}. These peaks can be attributed to the bending and stretching vibrations of the -OH bond in the crystal structure of magnesium hydroxide [20].

1-3. XRD of NC and MHMC

The XRD spectra of NC and MHMC are shown in Fig. 4. The mineralogical composition of NC was comprised primarily of clinoptilolite (2θ: 22°, 23°, 28°) and additionally of montmorillonite, quartz and feldspar by means of XRD [8]. Compared to XRD of NC, XRD of MHMC contained the peak of magnesium hydroxide (2θ: 38°) [21]. The XRD result was in agreement with the FTIR analysis.

2. Effect of Initial pH Value on MO and Cd^{2+} Adsorption in a Single Adsorption System

One of the most important factors in adsorption studies is the

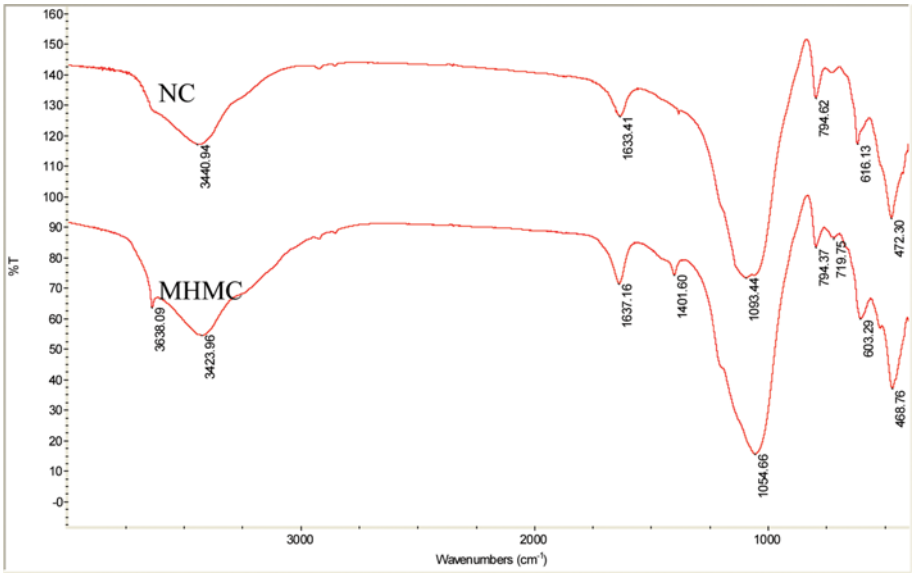

Fig. 3. FT-IR spectrum of NC and MHMC.

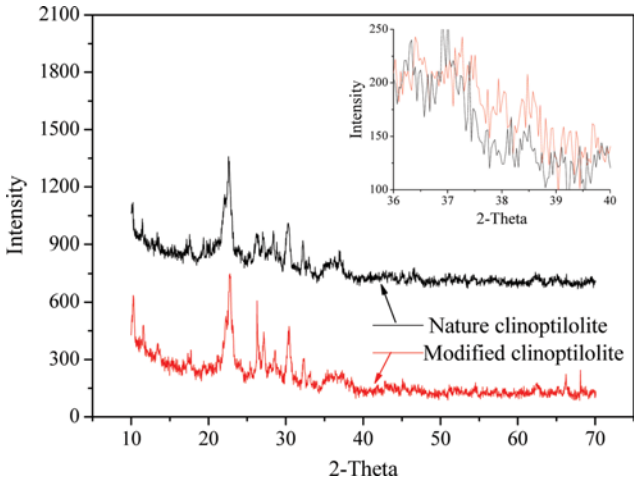

Fig. 4. The XRD spectra of NC and MHMC.

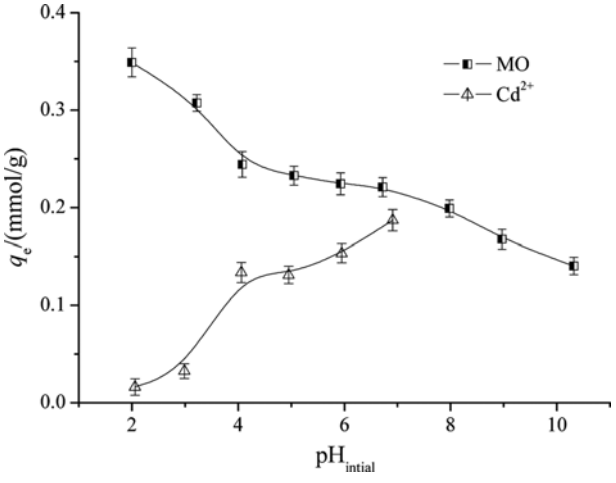

Fig. 5. Effect of solution pH on MO and Cd^{2+} on MHMC ($C_{0,Cd^{2+}}$= 0.36 mmol/L; $C_{0,MO}$=0.31 mmol/L; t=360 min, 298 K, MHMC dosage: 2 g/L).

effect of pH of the medium. The effect of initial pH of MO and Cd^{2+} was analyzed individually within the pH range of 2.0-10.3 and 2.1-7.00, respectively (Fig. 5). As can be seen from Fig. 5, the maximum adsorption capacity for MO onto MHMC was at pH 2.0. When the pH of solution changed from 2.0 to 10.3, the adsorption capacities decreased from 0.349 mmol/g to 0.140 mmol/g. The variation in MO uptake with respect to the initial solution pH can be explained on the basis of the structure of MO molecule and the pH_{pzc} of MHMC. When the pH of solution was lower than pH_{pzc}, the surface charge of MHMC was positive. The higher removal efficiency of MO may be due to neutralization of the negative charge at its surface as $-SO_3^-$ anion, which increased the protonation and the electrostatic attraction between the negatively charged $-SO_3^-$ anion and the positively charged adsorption site [22]. The increase in solution pH increased the number of hydroxyl groups, so decreased the number of positively charge sites and reduced the attraction between MO and MHMC. When the solution pH is above the pH_{pzc} value, the MHMC particle acquires a

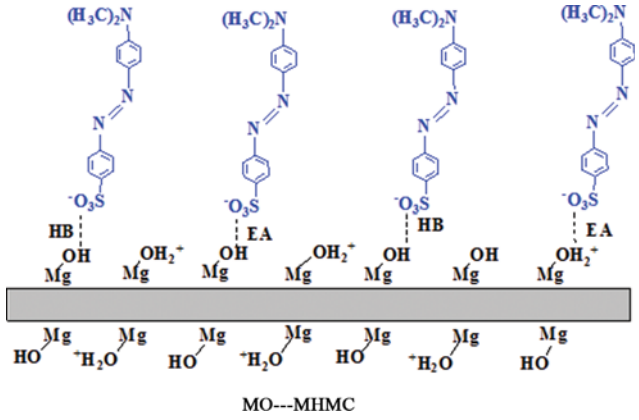

Scheme 2. Adsorption mechanism of MO on MHMC. The force of attraction between the hydrogen present in MHMC (-OH) and the oxygen present in the MO ($-SO_3^-$).
EA: Electrostatic attraction; HB: Hydrogen bonding.

negative surface charge. There was competition adsorption between the OH^- ions and the dye anions. Hence, the removal efficiency of the MO decreased with increasing the value of pH. But still a significant amount of MO removal was observed as the pH of the solution increased from 8.0 to 10.0. The result suggested that a hydrogen bond may be exist between the $-SO_3^-$ anion of MO and hydroxy contained in MHMC (Scheme 2).

For Cd^{2+}, on increasing the pH from 2.1 to 7.0, the adsorption capacity increased from 0.016 mmol/g to 0.19 mmol/g. The increase in the adsorption at higher pH may be attributed to two reasons. At low pH, the number of positively charged adsorbent sites increased, which did not favor the adsorption of positively charged Cd^{2+} ions due to electrostatic repulsion. Secondly, lower adsorption of Cd^{2+} at acidic pH is due to the presence of excess H^+ ions competing with Cd^{2+} for the adsorption sites of MHMC [23].

3. Adsorption Equilibrium Isotherms

Equilibrium data is significant for the design of adsorption system. In this work, the Langmuir, Freundlich, and Dubinin-Radushkevich models were applied to describe the adsorption equilibrium.

The Langmuir adsorption isotherm [24], as widely applied to describe experimental adsorption data, is given as:

$$q_e = \frac{q_m K_L C_e}{1 + K_L C_e} \quad (4)$$

where C_e is the concentration of adsorbate (mmol/L) at equilibrium, q_e is the amount of solute adsorbed at equilibrium (mmol/g), q_m (mmol/g) and K_L (L/mmol) are Langmuir constants related to adsorption capacity and energy of adsorption.

The Freundlich model [25] proposes a monolayer sorption with a heterogeneous energetic distribution of active sites. It assumes that an interaction between the adsorbed molecules takes place, can be expressed as:

$$q_e = K_F C_e^{1/n} \quad (5)$$

where K_F ((mmol/g)(L/mmol)$^{1/n}$) is the Freundlich constant which is correlated with the capacity of adsorption and 1/n is an indicator of adsorption intensity, and the value of the empirical parame-

ter 1/n (0.1<1/n<1), indicates favorable adsorption [26].

The Dubinin-Radushkevich model is generally applied to express the adsorption mechanism with the characteristic porosity and the apparent free energy. The non-line presentation of Dubinin-Radushkevich isotherm equation [27] is as follows:

$$q_e = q_m \exp(-\beta\varepsilon^2) \tag{6}$$

where q_e is the amount of adsorbate molecules adsorbed on per unit weight of adsorbent (mmol/g), q_m is the maximum adsorption capacity (mmol/g), β is the activity coefficient related to adsorption mean free energy mol^2/J^2, and ε is the Polanyi potential [28] given by:

$$\varepsilon = RT\ln\left(1+\frac{1}{C_e}\right) \tag{7}$$

E per molecule of adsorbate (of removing a molecule from its location in the space to the infinity) can be computed by the relationship:

$$E = \frac{1}{\sqrt{2\beta}} \tag{8}$$

The parameter gives information about the type of adsorption mechanism as a chemical ion-exchange or a physical adsorption. If the magnitude of E is between 8 and 16 kJ/mol, the sorption process is supposed to proceed via chemisorption, while for values of E <8 kJ/mol, the sorption process is of a physical nature.

The relative parameters for isotherm and kinetic equation were calculated employing the χ^2 between the experimental data and calculated data using non-linear regression analysis. The expression for χ^2 can be given as:

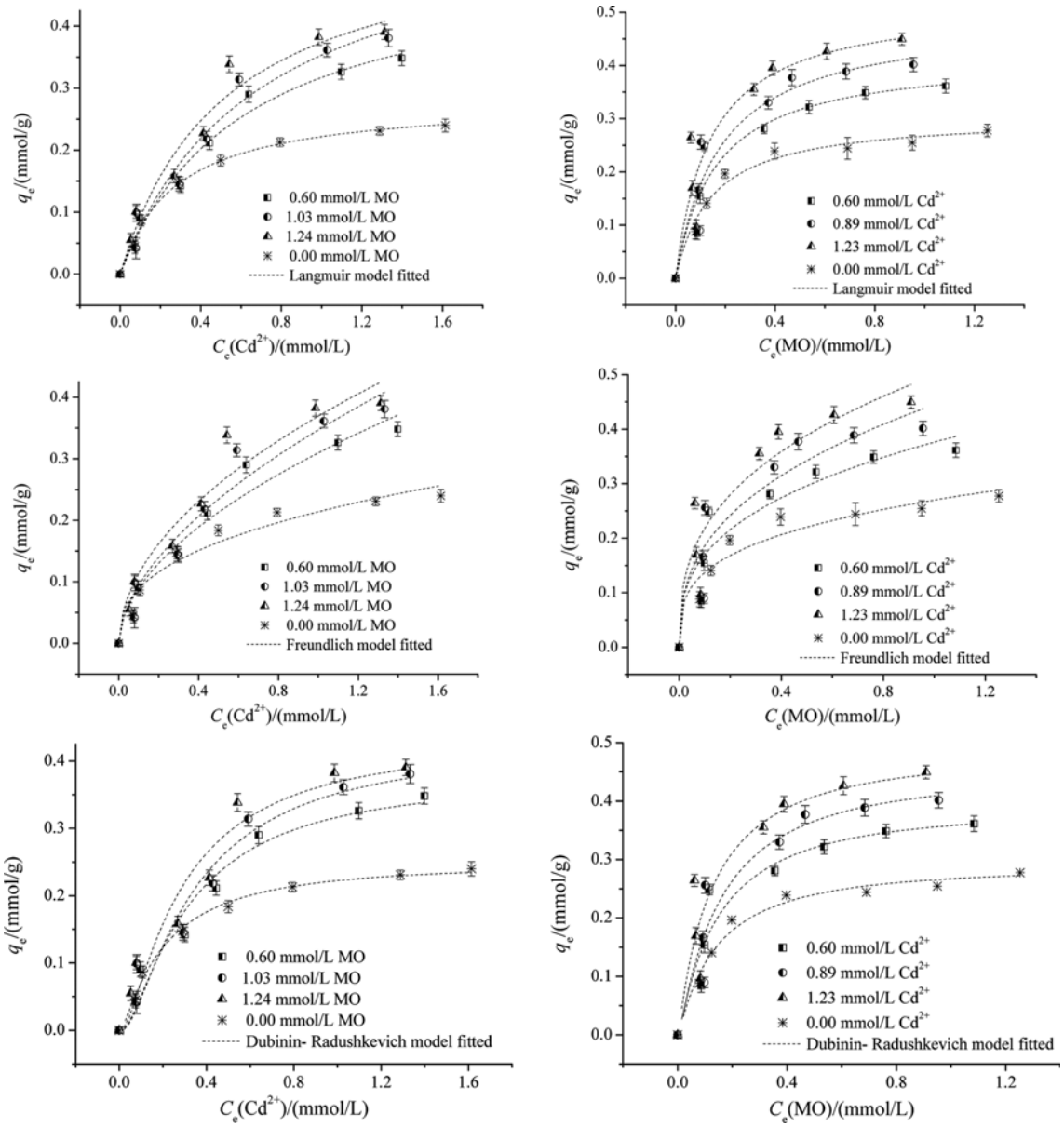

Fig. 6. Adsorption isotherms of MO and Cd^{2+} on MHMC in single and binary systems using non-linear regressive methods (MHMC dosage: 2.0 g/L; t=360 min; 298 K).

$$\chi^2 = \sum \frac{(q_{e,\,exp.} - q_{e,\,calc.})^2}{q_{e,\,calc.}} \quad (9)$$

where $q_{e,calc.}$ is the calculated adsorption capacity of MO or Cd^{2+} adsorbed onto MHMC, which is correlated with the various adsorption models and $q_{e,exp.}$ is correlated with the experimental data of adsorption capacity.

3-1. Adsorption Isotherms for the Single System

Fig. 6 illustrates the adsorption isotherms of MO and Cd^{2+} in single systems. The isotherms rise steeply at low liquid phase concentration, indicating completion adsorption with a plateau formed when the maximum adsorption capacity was achieved. This suggests that a saturation adsorbate monolayer was established.

Langmuir, Freundlich, and Dubinin-Radushkevich models have been used to describe the experimental data of adsorption isotherms. The parameters of the three models calculated on the basis of Eqs. (4), (5) and (6) are listed in Table 1. It can be seen that regression coefficients R^2 obtained from the Langmuir and Dubinin-Radushkevich models were bigger than that of the Freundlich model for MO and the values of χ^2 were lower, which suggests both the Langmuir and Dubinin-Radushkevich models appeared to be the better models for the adsorption of MO onto MHMC. However,

Table 1. Parameters for adsorption isotherms of adsorbates on MHMC in single or binary systems

Adsorbate	MO				Cd^{2+}			
C_0/mmol·kg^{-1}	$C_{0,\,Cd^{2+}}$/mmol/L				$C_{0,\,MO}$/mmol/L			
	0	0.60	0.89	1.23	0	0.60	1.03	1.24
Langmuir isotherm								
q_m/(mmol/g)	0.305	0.418	0.491	0.52	0.282	0.511	0.596	0.566
K_L/(L/mmol)	7.03	6.29	5.61	7.22	3.71	1.63	1.45	1.94
R^2	0.981	0.925	0.915	0.891	0.995	0.983	0.969	0.967
$\chi^2\times10^3$	0.80	1.53	2.27	3.51	0.40	0.36	0.77	0.88
Freundlich isotherm								
K_F (mmol/g) (L/mmol)$^{1/n}$	0.270	0.376	0.445	0.499	0.182	0.310	0.357	0.369
1/n	0.29	0.35	0.38	0.36	0.34	0.54	0.57	0.51
R^2	0.941	0.899	0.890	0.885	0.953	0.965	0.955	0.952
$\chi^2\times10^3$	0.24	2.05	2.94	3.69	0.49	0.71	1.12	1.30
Dubinin- Radushkevich isotherm								
q_m/(mmol/g)	0.287	0.386	0.445	0.479	0.247	0.374	0.421	0.428
E/(kJ/mol)	4.22	4.46	4.34	4.78	3.66	2.98	2.86	3.15
R^2	0.984	0.927	0.917	0.889	0.995	0.968	0.952	0.949
$\chi^2\times10^3$	0.46	1.50	2.22	3.56	0.30	0.65	1.20	1.39

Table 2. The comparison of adsorption capacities of MO and Cd^{2+} onto various adsorbent from the literature

Adsorbate	q_m/(mmol/g)	Adsorbent	References
MO	0.278	Modified clinoptilolite	This paper
	0.103	Bentonite	[47]
	0.273	Carbon coated monolith	[48]
	0.110	Anaerobic sludge	[49]
	0.322	Quaternary ammonium polyethylenimine modified silica	[50]
	2.70	Hierarchical nano/micro-structured Zn-Mg-Al layered double hydroxides	[51]
	0.064	Banana peel	[52]
	0.062	Orange peel	[52]
	0.157	Ficus caria fiber	[53]
Cd^{2+}	0.270	Modified clinoptilolite	This paper
	0.034	Raw corn stalk	[54]
	0.250	Hetero-atom functional mesoporous silica	[55]
	0.051	Banana peels	[56]
	0.312	Activated alumina	[57]
	0.253	Sewage sludge	[58]
	0.163	Al_{13}-pillared acid-activated montmorillonite	[59]

for Cd^{2+}, regarding the regression coefficients R^2, all the three models seem to be fit for the adsorption of Cd^{2+} onto MHMC. Therefore, it indicates that after adsorption, MO or Cd^{2+} monolayer covered the surface of adsorbent. From Table 1, one can see that the values of 1/n (0.1<1/n<1) indicating the adsorption behavior of MHMC were favorable for the MO and Cd^{2+} in single system. The values of E were lower than 8 kJ/mol for MO and Cd^{2+}, respectively, indicating that the nature of adsorption may contain physical adsorption process.

The value of q_m obtained from Langmuir isotherm of MO and Cd^{2+} is 0.305 and 0.282 mmol/g, respectively. This result indicates that the functional groups on the surface of MHMC had a relatively stronger affinity for MO than Cd^{2+}.

Part of the data on MO and Cd^{2+} adsorption capacity (values of q_m derived from the Langmuir equation) of various adsorbents is summarized in Table 2. Although the values of adsorption capacities were obtained at different experiment conditions, the results show that MHMC can be considered as a promising adsorbent for the removal of MO and Cd^{2+} from aqueous solutions.

3-2. Adsorption Isotherms for the Binary System

The adsorption isotherms in binary adsorption system of MO/Cd^{2+} and the fitted curves by the Langmuir, Freundlich and Dubinin-Radushkevich models of MO and Cd^{2+} are shown in Fig. 6. On the basis of the values of R^2, χ^2 and the experimental results showed in Table 1, both the Langmuir and Dubinin-Radushkevich models appear to be the better models for the adsorption of MO onto MHMC in binary adsorption system. For Cd^{2+}, all the three models seem to be fit for the adsorption of Cd^{2+} onto MHMC in binary system. The calculated *E* values for our system (Table 1) hint to the physical nature of the adsorption of MO and Cd^{2+} onto MHMC.

The adsorption capacity of MO increased with the initial concentration increasing under a fixed concentration of Cd^{2+} in the mixture solution and the tendency was the same as that of the single adsorption system. However, there is a novel phenomenon in the MO/Cd^{2+} binary adsorption system; the equilibrium uptake of MO onto MHMC increased continuously with an increase of the initial Cd^{2+} concentration. From Fig. 6, the initial concentration of Cd^{2+} was increased from 0.604 to 1.227 mmol/L, the adsorption capacity of MO was increased from 0.418 to 0.520 mmol/g in the MO/Cd^{2+} binary solution (Table 1). The same facilitated phenomenon was also found when Cd^{2+} was the target component. When the initial concentration of MO increased from 0.603 to1.242 mmol/L, the adsorption capacity of Cd^{2+} increased from 0.511 to 0.566 mmol/g. The higher adsorption capacity in binary system validated the synergism effect between Cd^{2+} and MO. The synergism effect caused by the two species could be observed evidently from Fig. 6 and Table 1. As to the uptake capacity of MO and Cd^{2+}, comparing the profiles of the single and binary systems, the latter were always higher during the experimental processes.

The synergism or competition among the dyes and heavy metals onto adsorbent can affect the mobility and the efficiency with which they can be removed from multicomponent solutions. Equilibrium distribution coefficient (K_d) can be used for the evaluation of selectivity and affinity of adsorbent MHMC for MO and Cd^{2+} in solution. The K_d values obtained from this study for MO or Cd^{2+} in MO/Cd^{2+} binary solution system are shown in Fig. 7. High

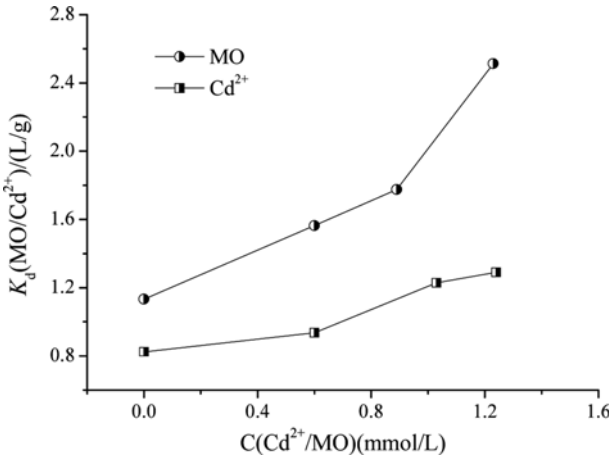

Fig. 7. The distribution coefficients K_d (mmol/g) of MO or Cd^{2+} in binary system.

values of K_d indicate that the dye or heavy metal has been retained by the solid phase through sorption reactions, while low values of K_d indicate that a large fraction of the dye or metal remains in solution [29].

In Fig. 7 the K_d (MO) values increased obviously with the concentration of Cd^{2+} increasing from 0 to 1.23 mmol/L; the same tendency was observed for the values of K_d (Cd^{2+}) increasing with the concentration of MO increasing from 0 to 1.24 mmol/L. According to the distribution coefficient (K_d), the sequence of adsorption affinity of MO and Cd^{2+} toward MHMC was found to be the following: K_d (MO) binary>K_d (Cd^{2+}) binary>K_d (MO) single>K_d (Cd^{2+}) single, indicating that MO was stronger adsorbed by MHMC than Cd^{2+} in binary metal system. These results show that the presence of Cd^{2+} or MO has an important advancement effect on the uptake of MO or Cd^{2+} in binary system.

In general, a mixture of different adsorbates may exhibit three types of behavior: synergism, antagonism and non-interaction. In MO/Cd^{2+} binary system, the presence of Cd^{2+} promoted the adsorption capacity of MO; the same trend is also observed for Cd^{2+}, which suggests that the adsorption system of MO/Cd^{2+} presented a synergistic effect, not competitive adsorption. The increase in Cd^{2+} adsorption efficiency can be explained by that the abundant MO molecules attract to the surface of MHMC due to electrostatic attraction (Eq. (10)). The positive electrostatic charges on the MHMC surface will be neutralized, which would reduce electrostatic repulsion between MHMC and Cd^{2+}. Meanwhile, the Cd^{2+} could be adsorbed on the MHMC surface through complexation (Eq. (11)) [30] or ion exchange (Eq. (12) and Eq. (13)) [30]; then the MHMC surface adsorbed Cd^{2+} have positive charges, which would serve as the sites for electrostatic attraction to negative charged of MO as shown in Eq. (14) and Eq. (15). On the other hand, there may exist the hydrogen bonding between the $-SO_3^-$ group of MO and the hydrated cadmium ions, so MO-cadmium complexes may be formed in binary systems. Through the complexation or ion exchange between MHMC and Cd^{2+}, Cd^{2+} could attached to the surface of MHMC individually or bound by the MO-cadmuim complex as shown in Eq. (16), which also results in an increase in adsorption capacity. Scheme 3 shows the likely molecular arrangements of

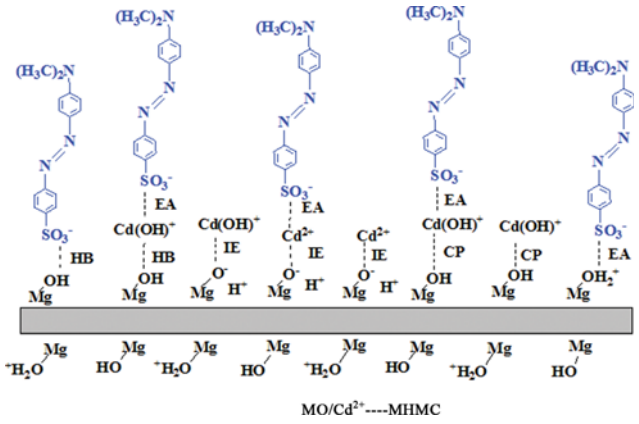

Scheme 3. MO and Cd^{2+} adsorption on MHMC in binary system. EA: Electrostatic attraction; HB: Hydrogen bonding; IE: Ion exchange; CP: Complexation.

adsorption of Cd^{2+} and MO on MHMC. The complex reactions of Cd^{2+} and MO with magnesium hydroxide may be written as follows [31]:

$$\equiv MgOH_2^+ + MO^- \rightleftharpoons \equiv MgOH_2^+ \text{ --- } MO^- \quad (10)$$

$$\equiv MgOH + Cd^{2+} + H_2O \rightleftharpoons \equiv [MgOH\text{---}CdOH]^+ + H^+ \quad (11)$$

$$\equiv MgOH + Cd^{2+} \rightleftharpoons \equiv MgOCd^+ + H^+ \quad (12)$$

$$\equiv MgOH + Cd^{2+} + H_2O \rightleftharpoons \equiv MgOCdOH^+ + H^+ \quad (13)$$

$$\equiv MgOH + Cd^{2+} + MO^- + H_2O \rightleftharpoons \equiv [MgOH\text{---}CdOH]^+\text{---}MO^- + H^+ \quad (14)$$

$$\equiv MgOH + Cd^{2+} + MO^- \rightleftharpoons \equiv MgOCd^+\text{---}MO^- + H^+ \quad (15)$$

$$\equiv MgOH + Cd^{2+} + H_2O + MO^- \rightleftharpoons \equiv MgOCdOH\text{---}MO + H^+ \quad (16)$$

4. Adsorption Kinetics

To interpret the experimental data, it is necessary to identify the step that controlled the overall rate in adsorption processes. In this study, five kinetic models including pseudo-first-order model, pseudo-second-order model, Elovich model, the intra-particle diffusion model and Bangham's equation were used to investigate the mechanism of adsorption and potential rate controlling steps such as chemical reaction, diffusion control and mass transport processes.

The pseudo-first-order model [32] has been widely employed to predict adsorption kinetics. The model is given as follows:

$$q_t = q_e(1 - e^{-k_1 t}) \quad (17)$$

where q_e is the adsorbate adsorption capacity at equilibrium, while q_t is the adsorbate adsorption capacity at time (min), and k_1 (min^{-1}) is the pseudo-first-order rate constant.

The pseudo-second-order kinetic model [33] can be written as the following equation:

$$q_t = \frac{k_2 q_e^2 t}{1 + k_2 q_e t} \quad (18)$$

where k_2 (g $mmol^{-1}$ min^{-1}) is the pseudo-second-order rate constant.

The Elovich kinetic equation [34] is given by the following equation:

$$q_t = A + B \ln t \quad (19)$$

where A and B are the Elovich kinetic model constants.

The adsorbate transport from the solution phase to the surface of the adsorbent particles occurs in several steps. The overall adsorption process may be controlled either by one or more steps, e.g., film or external diffusion, pore diffusion, surface diffusion and adsorption on the pore surface, or a combination of more than one step. The possibility of intra-particle diffusion was explored by using the intra-particle diffusion model [35]:

$$q_t = k_{id} t^{1/2} + C \quad (20)$$

where k_{id} (mmol/g $min^{0.5}$) is the intra-particle diffusion rate constant and C (mmol/g) is a constant related to the thickness of the boundary layer, which is in direct ratio to the effect of the boundary layer.

Bangham's equation can be further employed to check whether pore diffusion was the only rate-controlling step or not in the adsorption system. If this equation is an adequate representation of experimental data, the adsorption kinetics is limited by pore diffusion [36]. Bangham's equation is given as:

$$\log\log\left(\frac{C_0}{C_0 - q_t m}\right) = \log\left(\frac{k_0 m}{2.303 v}\right) + \alpha \log t \quad (21)$$

where C_0 is initial concentration of adsorption of adsorbate in solution (mmol/L), v is the volume of solution (L), m is the weight of adsorbent used per liter of solution (g/L), q_t (mmol/g) is the amount of adsorbate retained at time t, and α (<1), k_0 is constant.

4-1. Single System of MO and Cd^{2+}

The effect of contact time on the amount of adsorbed in single system of MO and Cd^{2+} is shown in Fig. 8: the adsorption rate was rapid at first 100 min, after which the rate slowed down and the equilibrium was reached in 360 min contact time. The relative parameters of three kinetic models (pseudo-first-order model, pseudo-second-order model and Elovich model) and values of R^2, χ^2 using nonlinear regressive method for adsorption of MO and Cd^{2+} onto MHMC are listed in Table 3.

All three models have a high value of R^2 and low value of χ^2 for MO in the single system, which shows that the pseudo-first-order model, pseudo-second-order model and the Elovich model can be

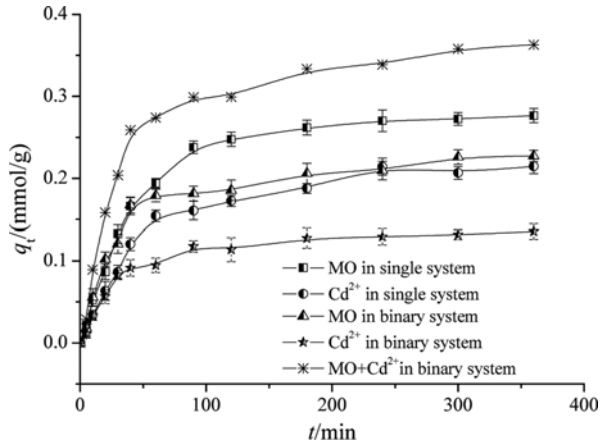

Fig. 8. Effect of contact time on the amount of adsorbed in single and binary systems (MHMC dosage: 2.0 g/L; 298 K; pH=7; Single system: $C_{0(MO)}=C_{0(Cd2+)}=1.2$ mmol/L; binary system: $C_{0(MO)}=C_{0(Cd2+)}=0.60$ mmol/L).

Table 3. Parameters for adsorption kinetics of adsorbates on MHMC in single and binary systems

Adsorbate	MO		Cd^{2+}	
	Single	Binary	Single	Binary
Pseudo-first-order model				
$q_{e,exp}$/(mmol/g)	0.277	0.227	0.215	0.136
$q_{e,calc}$/(mmol/g)	0.272	0.211	0.207	0.128
$k_1\times10^2$ (min^{-1})	2.15	3.06	1.90	2.86
R^2	0.996	0.976	0.988	0.984
$\chi^2\times10^2$	0.34	1.34	0.61	0.64
Pseudo-second-order model				
$q_{e,exp}$/(mmol/g)	0.277	0.227	0.215	0.136
$q_{e,calc}$/(mmol/g)	0.319	0.242	0.246	0.147
$k_2\times10^2$ (g/mmol min)	7.62	15.1	8.37	23.70
R^2	0.989	0.980	0.988	0.987
$\chi^2\times10^2$	1.33	1.77	0.98	0.86
Elovich model				
A	−0.088	−0.043	−0.075	−0.027
B	0.066	0.048	0.051	0.029
R^2	0.976	0.966	0.982	0.973
$\chi^2\times10^2$	1.77	4.70	2.02	1.18
Intra-particle diffusion model				
$k_{i1}\times10^2$/(mmol/g $min^{1/2}$)	3.06	3.02	2.57	1.43
$C_1\times10^2$ (mmol/g)	−4.28	−4.11	−4.68	−0.99
R_1	0.994	0.983	0.995	0.965
$SD_1\times10^2$	0.97	1.27	0.557	1.08
$k_{i2}\times10^3$/(mmol/g $min^{1/2}$)	4.04	4.86	5.87	2.16
$C_2\times10^2$ (mmol/g)	20.34	13.72	10.89	9.50
R_2	0.972	0.987	0.965	0.938
$SD_2\times10^2$	0.42	0.392	0.73	0.330
Bangham's model				
α	0.623	0.626	0.627	0.5544
$K_0\times10^2$ (L/g)	1.15	2.42	0.77	1.60
R^2	0.895	0.861	0.908	0.832
SD	0.134	0.158	0.125	0.156

SD: standard deviation

used for predicting the kinetic process of MO adsorption on MHMC in the experimental conditions. However, the values of R^2 and χ^2 show that the pseudo-first-order model and pseudo-second-order model were better fitted than that of the Elovich model for the adsorption of Cd^{2+} on MHMC. The results indicate that the adsorption process of MO and Cd^{2+} include chemisorption and physisorption. The values of $q_{e,calc}$ calculated by pseudo-first-order model for MO (0.272 mmol/g) and Cd^{2+} (0.207 mmol/g) agreed better with the experimental $q_{e,exp}$ values ($q_{e,exp}$(MO)=0.277 mmol/g, $q_{e,exp}$(Cd^{2+})=(0.215 mmol/g) than those from the pseudo-second-order model ($q_{e,calc}$(MO)=0.319 mmol/g, $q_{e,calc}$(Cd^{2+})=0.246 mmol/g) in single systems, respectively. The removal effective is in the order of MO>Cd^{2+}. This result is also consistent with the foregoing conclusion derived from the Langmuir model.

Adsorption kinetics is usually controlled by different mechanisms. To gain insight into the mechanisms and rate controlling steps affecting the kinetics of adsorption, the kinetic experimental results were fitted to the intraparticle diffusion model. The intra-particle diffusion model implies that the plot of q_t values $t^{1/2}$ should be linear. If the line passed through the origin, the intra-particle diffusion would be the sole rate limiting step. If the line did not pass through the origin, it implies that intra-particle diffusion was not the sole rate control step, and other processes may control the adsorption rate [37]. The plot of q_t versus $t^{0.5}$ for MO and Cd^{2+} adsorption on MHMC in single system is shown in Fig. 9, and the values of k_{id} and C are listed in Table 3. From Fig. 9, the experimental data points show two linear sections, which indicates the adsorption processes have two steps. The first linear segments did not pass through the origin, suggesting that pore diffusion was not the sole rate limiting step. The result indicates the mechanism of dyes

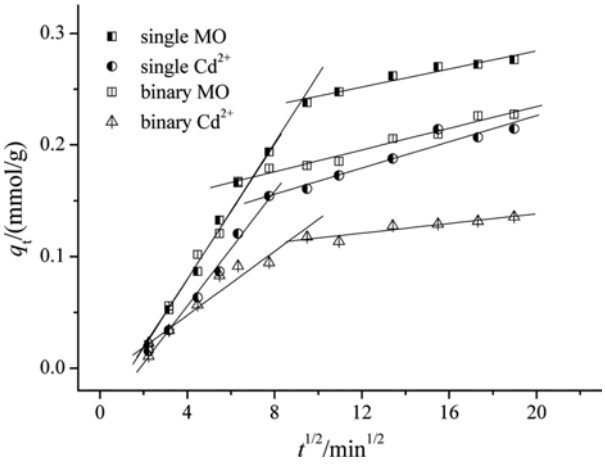

Fig. 9. Intra-particle diffusion plots for single and binary systems onto MHMC (MHMC dosage: 2.0 g/L; 298 K; pH=7).

and Cd^{2+} adsorption is complex and the actual process may contain surface adsorption and intra-particle diffusion for MO and Cd^{2+} in the single system. Table 3 indicates that the order of adsorption rate is $k_{d1}(MO)>k_{d1}(Cd^{2+})$ in single systems, which suggests that the existence of electrostatic repulsion affected the diffusion rate of Cd^{2+} from solution to the surface of MHMC. Meanwhile, it can be seen from Table 3, the value of $k_{d2}(Cd^{2+})$ was bigger than that of $k_{d2}(MO)$, which indicates that the smaller ion radius size of Cd^{2+} may be enhance the diffusion rate into the internal pore structure of MHMC.

Bangham's plot for MO and Cd^{2+} adsorption on MHMC in single system is shown in Fig. 10, and the values of k_0 and α are listed in Table 3. The experimental data put to representation by Eq. (20) did not give a good fit to the model data as expressed in Fig. 10. This indicates that the diffusion of the adsorbate into the pores of the adsorbents is not the only rate controlling step [38].

To corroborate the actual rate controlling steps in MO and Cd^{2+} adsorption on MHMC, the experimental data was further analyzed by the following equation [39]:

$$D_i = \frac{0.03r^2}{t_{1/2}} = 0.03k_2q_e r^2 \quad (22)$$

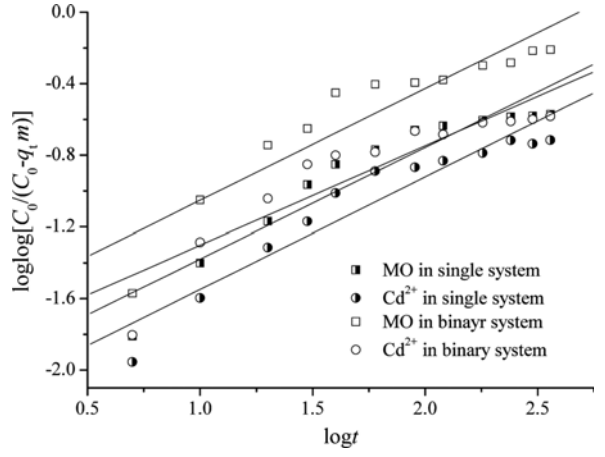

Fig. 10. Bangham's plot for single and binary systems onto MHMC (MHMC dosage: 2.0 g/L; 298 K; pH=7).

where k_2 and q_e can be obtained from Table 3, r is the radius of the adsorbent particle in centimeters and D_i (20-40 mesh, 30 mesh was chosen) is the diffusion coefficient value for the intraparticle transport of MO and Cd^{2+} in cm^2/s. According to Singh et al. [40], a value of D_i of the order of 10^{10}-10^{11} cm^2/s indicates that intraparticle diffusion is the rate limiting step in the adsorption process. In this study, the values of D_i for MO and Cd^{2+} were 4.57×10^{-8} and 3.87×10^{-8} cm^2/s, respectively, which is larger than 3-4 orders of magnitude. This indicates that the intraparticle diffusion is not the rate-controlling step.

4-2. Binary Component of MO and Cd^{2+}

The kinetic result of MO and Cd^{2+} in a binary system is also shown in Fig. 8. The adsorption capacity of MO or Cd^{2+} increased with the time increasing, followed by a plateau, which was the same phenomenon as single adsorption system. Compared with the adsorption capacity of MO and Cd^{2+} in the single system, the higher total adsorption capacity in the binary adsorption system was observed from Fig. 8.

The relative parameters of three kinetic models and values of R^2, χ^2 for the binary system are listed in Table 3. It can be seen that the values of R^2 obtained from the pseudo-first-order model and pseudo-second-order mode were higher than that of the Elovich model, which suggests that the pseudo-first-order model and pseudo-second-order mode appear to be suitable for the adsorption of MO or Cd^{2+} onto MHMC in binary system.

Fig. 9 shows the fitted curves of the intraparticle diffusion model of MO and Cd^{2+} in binary adsorption systems. The adsorption of MO and Cd^{2+} shows two stage diffusion processes, which was the same as the single system. It suggests the adsorption process of MO and Cd^{2+} may contain the surface adsorption and intraparticle diffusion in the MO/Cd^{2+} binary system. From Table 3, the value of $k_{t1}(MO)$ was greater than that of $k_{t1}(Cd^{2+})$ in binary system, which indicates MO still exhibited higher diffusion rate than Cd^{2+}. It was because the electrostatic attraction between MO and MHMC enhanced the diffusion rate. However, the value of $k_{t2}(MO)$ was also slightly greater than that of Cd^{2+}, which was different from the single system. The reason may be that MO-cadmium complex exists in the binary system and the bigger molecule size of the complex could impede the diffusion from the surface into the internal pore structure of MHMC. In a binary system, the values of D_i for MO and Cd^{2+} were 6.87×10^{-8} and 6.55×10^{-8} cm^2/s, respectively. It indicates that the intraparticle diffusion is not the rate controlling step.

Bangham's plot for MO and Cd^{2+} in binary adsorption system is shown in Fig. 10. The values of k_0 and α are also listed in Table 3. The results show that the model did not match experimental data, so the diffusion in the pores of MHMC was not only rate controlling.

The values of q_m calculated by pseudo-first-order model and pseudo-second-order model were all in the order of MO>Cd^{2+}, which shows that MHMC has a stronger adsorption affinity to MO than Cd^{2+}. It is no surprise for such a phenomenon, MO is an anionic dye; thus electrostatic attraction could result in strong adsorption of MO on MHMC. Another reason is that there may exist a hydrogen bond between -SO_3^- (from MO) and -OH (from MHMC). Although Cd^{2+} ion has a smaller radius size, MHMC has a stronger adsorption affinity to MO than Cd^{2+}. However, the total adsorption capacity of MO and Cd^{2+} on MHMC was higher

than that of the adsorption capacity of MO and Cd^{2+} at equilibrium in single adsorption system, which suggests that MHMC can be used as an adsorbent for removal of dyes and heavy metal in the multi-solute system. The likely molecular arrangements of adsorption of MO and Cd^{2+} on the MHMC in binary solution are shown in Scheme 3.

CONCLUSION

MHMC showed a high adsorption capacity for MO and Cd^{2+} ions from single and binary solutions, and the adsorption capacity followed the order of MO>Cd^{2+}. The maximum adsorption amounts in single system were 0.305 and 0.282 mmol/g for MO and Cd^{2+}, respectively. In the binary system of MO/Cd^{2+}, the equilibrium adsorption capacities of MO and Cd^{2+} increased as compared to single systems, which indicated that the adsorption system presented a synergistic effect, not antagonistic interaction between MO and Cd^{2+} on MHMC. Experimental adsorption data from single and binary systems were successfully described by the Langmuir and Dubinin-Radushkevich equilibrium isotherm models, which may indicate that the number of adsorption sites available for MO and Cd^{2+} on MHMC is limited, and that an adsorbate monolayer was established at saturation. The adsorption kinetic studies showed that the adsorption process followed pseudo-first-order model and pseudo-second-order model in single and binary systems, which indicated that the adsorption process of MO and Cd^{2+} included chemisorption and physisorption. The process mechanism of MO and Cd^{2+} adsorption was found to be complex, consisting of both surface adsorption and pore diffusion with chemical process in the single and binary systems.

ACKNOWLEDGEMENTS

This work was supported by the Education Department of Henan Province in China (No. 2010A610003) and Henan Science and Technology Department in China (No. 122300410163).

REFERENCES

1. I. D. Mall, V. C. Srivastava and N. K. Agarval, *Dyes Pigm.*, **69**, 210 (2006).
2. E. Alver and A. Ü. Metin, *Chem. Eng. J.*, **200-202**, 59 (2012).
3. A. Kongsuwan, P. Patnukao and P. Pavasant, *J. Ind. Eng. Chem.*, **15**, 465 (2009).
4. Y. Al-Degs, M. A. M. Khraisheh, S. J. Allen, M. N. Ahmad and G. M. Walker, *Chem. Eng. J.*, **128**, 163 (2007).
5. T. Sismanoglu, Y. Kismir and S. Karakus, *J. Hazard. Mater.*, **184**, 164 (2010).
6. C. Y. Cao, J. Qu, F. Wei, H. Liu and W. G. Song, *ACS Appl. Mater. Inter.*, **4**, 4283 (2012).
7. D. A. Kramer, *Kirk-Othmer Encyclopedia of Chemical Technology*, John Wiley & Sons, Inc. New Jersey, USA (2004).
8. W. H. Zou, H. J. Bai, L. Zhao, K. Li and R. P. Han, *J. Radioanal. Nucl. Chem.*, **288**, 779 (2011).
9. G. Z. Kyzas, N. K. Lazaridis and A. C. Mitropoulos, *Chem. Eng. J.*, **189-190**, 148 (2012).
10. R. P. Han, Y. Wang, Q. Sun, L. L. Wang, J. Y. Song, X. T. He and C. C. Dou, *J. Hazard. Mater.*, **175**, 1056 (2010).
11. J. Y. Song, W. H. Zou, Y. Y. Bian, F. Y. Su and R. P. Han, *Desalination*, **265**, 119 (2011).
12. R. P. Han, L. J. Zhang, C. Song, M. M. Zhang, H. M. Zhu and L. J. Zhang, *Carbohydr. Polym.*, **79**, 1140 (2010).
13. M. Şaban Tanyildizi, *Chem. Eng. J.*, **168**, 1234 (2011).
14. M. S. Rahman and M. R. Islam, *Chem. Eng. J.*, **149**, 273 (2009).
15. N. Gupta, A. K. Kushwaha and M. C. Chattopadhyaya, *J. Taiwan Inst. Chem. E.*, **43**, 125 (2012).
16. S. A. Ahmed, *Carbohydr. Polym.*, **83**, 1470 (2011).
17. V. Hernández-Montoya, M. A. Pérez-Cruz, D. I. Mendoza-Castillo, M. R. Moreno-Virgen and A. Bonilla–Petriciolet, *J. Environ. Manage.*, **116**, 213 (2013).
18. W. H. Zou, H. J. Bai and S. P. Gao, *J. Chem. Eng. Data.*, **57**, 2792 (2012).
19. P. C. C. Faria, J. J. M. Órfão and M. F. R. Pereira, *Water Res.*, **38**, 2043 (2004).
20. P. Y. Koh, *Deposition and assembly of magnesium hydroxide nanostructures on zeolite 4a surfaces*, Georgia Institute of Technology, Atlanta (2010).
21. T. H. Bae, J. Q. Liu, J. A. Thompson, W. J. Koros, C. W. Jones and S. Nair, *Micropor. Mesopor. Mater.*, **139**, 120 (2011).
22. D. Z. Shen, J. X. Fan, W. Z. Zhou, B. Y. Gao, Q. Y. Yue and Q. Kang, *J. Hazard. Mater.*, **172**, 99 (2009).
23. N. Buvaneswari and C. Kannan, *J. Hazard. Mater.*, **189**, 294 (2011).
24. I. Langmuir, *J. Am. Chem. Soc.*, **38**, 2221 (1916).
25. H. M. F. Freundlich, *J. Phys. Chem.*, **57**, 385 (1906).
26. A. S. Özcan, B. Erdem and A. Özcan, *J. Colloid Interface Sci.*, **280**, 44 (2004).
27. M. Auta and B. H. Hameed, *Chem. Eng. J.*, **171**, 502 (2011).
28. K. Y. Foo and B. H. Hameed, *Chem. Eng. J.*, **156**, 2 (2010).
29. A. A. El-Bayaa, N. A. Badawy and E. Abd AlKhalik, *J. Hazard. Mater.*, **170**, 1204 (2009).
30. J. W. Murray, *J. Colloid Interface Sci.*, **46**, 357 (1974).
31. K. Lackovic, M. J. Angove, J. D. Wells and B. B. Johnson, *J. Colloid Interface Sci.*, **269**, 37 (2004).
32. B. H. Hameed, A. A. Ahmad and N. Aziz, *Desalination*, **247**, 551 (2009).
33. M. J. Ahmed and S. K. Theydan, *Ecotox. Environ. Safe.*, **84**, 39 (2012).
34. A. Khaled, A. E. Nemr, A. El-Sikaily and O. Abdelwahab, *J. Hazard. Mater.*, **165**, 100 (2009).
35. N. Kannan and M. M. Sundaram, *Dyes Pigm.*, **51**, 25 (2001).
36. D. D. Maksin, A. B. Nastasović, A. D. Milutinović-Nikolić, L. T. Suručić, Z. P. Sandić, R. V. Hercigonja and A. E. Onjia, *J. Hazard. Mater.*, **209-210**, 99 (2012).
37. L. Liu, Y. Z. Wan, Y. D. Xie, R. Zhai, B. Zhang and J. D. Liu, *Chem. Eng. J.*, **187**, 210 (2012).
38. P. Barkakati, A. Begum, M. L. Das and P. G. Rao, *Chem. Eng. J.*, **161**, 34 (2010).
39. M. Doğan, Y. Özdemir and M. Alkan, *Dyes Pigm.*, **75**, 701 (2007).
40. K. K. Singh, R. Rastogi and S. H. Hasan, *J. Colloid Interface Sci.*, **290**, 61 (2005).